Chemical Science

ROYAL SOCIETY OF CHEMISTRY

EDGE ARTICLE

View Article Online
View Journal | View Issue

Cite this: *Chem. Sci.*, 2024, **15**, 17547

All publication charges for this article have been paid for by the Royal Society of Chemistry

Received 3rd July 2024
Accepted 26th September 2024

DOI: 10.1039/d4sc04387a

rsc.li/chemical-science

Metal–organic frameworks with two different-sized aromatic ring-confined nanotraps for benchmark natural gas upgrade†

Shu-Yi Li,[a] Ying-Ying Xue,[a] Jia-Wen Wang,[a] Hai-Peng Li,[a] Jiao Lei,[a] Hong-Juan Lv,[a] Xianhui Bu,*[b] Peng Zhang,[a] Ying Wang,[a] Wen-Yu Yuan[a] and Quan-Guo Zhai*[a]

Recovery of light alkanes from natural gas is of great significance in petrochemical production. Herein, a promising strategy utilizing two types of size-complementary aromatic ring-confined nanotraps (called bi-nanotraps here) is proposed to efficiently trap ethane (C_2H_6) and propane (C_3H_8) selectively at their respective sites. Two isostructural metal–organic frameworks (MOFs, SNNU-185/186), each containing bi-nanotraps decorated with six aromatic rings, are selected to demonstrate the feasibility of this method. The smaller nanotrap acts as adsorption sites tailored for C_2H_6 while the larger one is optimized in size for C_3H_8. The separation is further facilitated by the large channels, which serve as mass transfer pathways. These advanced features give rise to multiple C–H···π interactions and size/shape-selective interaction sites, enabling SNNU-185/186 to achieve high C_2H_6 adsorption enthalpy (43.5/48.8 kJ mol^{-1}) and a very large thermodynamic interaction difference between C_2H_6 and CH_4. Benefiting from the bi-nanotrap effect, SNNU-185/186 exhibits benchmark experimental natural gas upgrade performance with top-level CH_4 productivity (6.85/6.10 mmol g^{-1}), ultra-high purity and first-class capture capacity for C_2H_6 (1.23/0.90 mmol g^{-1}) and C_3H_8 (2.33/2.15 mmol g^{-1}).

Introduction

Natural gas is mainly composed of methane (CH_4, 85% by volume) which is an important clean energy source and essential chemical feedstock. However, the presence of ethane (9% C_2H_6) and propane (3% C_3H_8) not only reduces the combustion efficiency and conversion rate of CH_4, but also affects the safety of CH_4 storage.[1–5] In addition, C_2H_6 and C_3H_8 are valuable petrochemical feedstocks for the manufacture of alkenes and polymers.[6–11] Therefore, efficient separation and recovery of C_2H_6 and C_3H_8 from natural gas are important for both CH_4 upgrading and full energy utilization. The current separation process is mainly based on cryogenic distillation technology which is energy intensive and environmentally unfriendly.[12–14] By contrast, adsorption-based separation using solid adsorbents is cost- and energy-efficient.[15–20]

With guest accessible porosity, and a variety of different components contributing to the tunability of pore structures and surface properties, porous coordination polymers (PCPs) or metal–organic frameworks (MOFs) are a promising class of solid adsorbents capable of overcoming the performance bottleneck resulting from imprecise pore control, few structural building units, and a limited number of coordination pathways of traditional adsorbents.[21–25] To date, many MOFs have been investigated for $C_3H_8/C_2H_6/CH_4$ separation based on the thermodynamic separation mechanism. Generally, creating a polar pore surface (C–H···O/N/F hydrogen bonds)[26–30] or non-polar pore environments (aromatic C–H···π bonds or confined aliphatic C–H···C hydrogen bonds), and simultaneously regulating pore size to provide a confined space for enhanced MOF–gas interaction,[31–34] are effective strategies. One difficulty is that the performance of MOF materials is limited by the C_2H_6/CH_4 separation step as shown in Zn-BPZ-SA,[5] LIFM-ZZ-1,[9] BSF-2,[14] MIL-101,[30] UiO-66-NaPh[34] and CFA-1,[35] largely due to the greater similarity in molecular size and chemical properties between C_2H_6 and CH_4.[4,34] Another often-neglected but crucial reason is the competitive adsorption between C_3H_8 and C_2H_6 in the ternary gas separation system.[36] C_3H_8 molecules preferentially occupy adsorption sites to form stronger interaction with the framework due to their larger polarizability and molecular size compared to C_2H_6, which further increases the difficulty of the C_2H_6/CH_4 separation step. Therefore, the key to improving the

[a]*Key Laboratory of Applied Surface and Colloid Chemistry, Ministry of Education, School of Chemistry & Chemical Engineering, Shaanxi Normal University, Xi'an, Shaanxi, 710062, China. E-mail: zhaiqg@snnu.edu.cn*

[b]*Department of Chemistry and Biochemistry, California State University, Long Beach, California, 90840, USA. E-mail: xianhui.bu@csulb.edu*

† Electronic supplementary information (ESI) available. CCDC 2268660 and 2268661. For ESI and crystallographic data in CIF or other electronic format see DOI: https://doi.org/10.1039/d4sc04387a

performance of C_2H_6/CH_4 separation is to increase the thermodynamic difference between C_2H_6 and CH_4 while simultaneously installing size-selective sites for C_2H_6 and C_3H_8 to minimize the competitive adsorption between C_2H_6 and C_3H_8.

Fortunately, the difference in molecular polarizability and the number of H-donors between C_3H_8, C_2H_6, and CH_4 could enable thermodynamic preferential adsorption of C_3H_8 or C_2H_6 by creating polar/non-polar pore surfaces. Compared to single adsorption sites, nanotraps or molecular traps that allow for the selective capture of specific gas molecules are more effective and attractive.[37–45] With multiple and gas-specific adsorption sites, nanotraps provide stronger binding interactions and recognition capabilities for target molecules, which is promising for widening the thermodynamic gap between C_3H_8, C_2H_6 and CH_4. However, the construction of nanotraps is rare and challenging for MOFs.

In addition, the combination of strong binding affinity and molecular sieving should have great potential in preventing competitive adsorption and achieving the most effective purification and separation. Its high efficiency and application potential have been demonstrated in multi-component separation.[36,46–48] The construction of coexistent C_2H_6- and C_3H_8-selective adsorption sites in one MOF system is difficult because C_2H_6 and C_3H_8 tend to occupy the same sites, with C_3H_8 being preferred. However, utilizing the difference in kinetic diameter between C_3H_8 (5.1 Å) and C_2H_6 (4.4 Å) to discriminate between them could be an effective method to eliminate competitive adsorption (Table S1†), leading to enhanced MOF performance in the key C_2H_6/CH_4 step. Overall, the combination of nanotraps with the molecular sieving effect is expected to facilitate multiple and strong interactions and widen the thermodynamic difference between C_3H_8, C_2H_6 and CH_4. It will also help install sites targeting selective adsorption for C_3H_8 and C_2H_6 to reduce their competitive adsorption and, therefore, maximize the separation performance (Scheme 1).

Herein, a promising example of bi-nanotraps is demonstrated. In two newly constructed MOFs (SNNU-185/186), the smaller type of nanotraps with appropriate size and shape is ideally suited for accommodating C_2H_6 based on the thermodynamic-molecular sieving mechanism and the larger nanotraps are more advantageous for trapping C_3H_8 thanks to the thermodynamic interaction difference. In the meantime, the large channels serve as mass transfer pathways, promoting gas molecules to enter the adsorption sites from pore walls. As a result, multiple C–H···π interactions and highly discriminating interaction sites are achieved in one unprecedented MOF system, contributing to benchmark $-Q_{st}$ for C_2H_6 and the exceptionally large $-Q_{st}$ difference between C_2H_6 and CH_4. The overall effect is greatly increased thermodynamic difference and weakened competitive adsorption. Together with excellent adsorption capability and high stability, SNNU-185 and SNNU-186 can produce ultra-high purity CH_4 (>99.9999%) at flow rates of 4/6 mL min^{-1} with top-level productivities for CH_4 (6.85 and 6.10 mmol g^{-1}), and top-notch capture capacities for C_2H_6 (1.23 and 0.90 mmol g^{-1}) and C_3H_8 (2.33 and 2.15 mmol g^{-1}) in breakthrough experiments. GCMC simulation provides a molecular level insight and mechanistic explanation of the role of bi-nanotraps. This work not only provides promising materials for natural gas upgrade, but also reveals an effective design philosophy toward the development of porous coordination polymers for challenging multi-component separation processes.

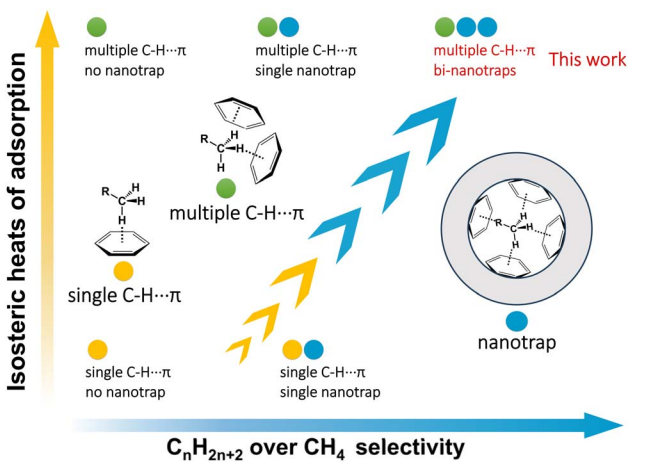

Scheme 1 A proposed strategy for paraffin separation with the synergistic effect of C–H···π interactions and nanotraps.

Results and discussion

Hydrothermal reactions of 1,3,5-tris(4-pyridyl)-benzene (TPB) or 2,4,6-tri(4-pyridinyl)-1-pyridine (TPP), 2,5-pyridinedicarboxylic acid (2,5-PDC) and cobalt acetate hydrate were used to synthesize SNNU-185 (with TPB) and SNNU-186 (with TPP) (Fig. S1 and S2†). From the single crystal analysis, they are found to be isostructural and crystallize in the hexagonal space group $P\bar{6}c2$ with the formula of $\{[Co_3(\mu_3\text{-OH})][Co(2,5\text{-PDC})_2]_3(TPB/TPP)_3\}_n$ (Fig. S3 and Table S2†), which is isostructural with our reported SNNU-54 (ref. 49) synthesized under different conditions (Fig. S4 and S5†). SNNU-185 and SNNU-186 were selected to demonstrate the feasibility of the aromatic ring-confined bi-nanotrap strategy for efficiently and separately trapping C_2H_6 and C_3H_8 based on a thermodynamic-molecular sieving coupling mechanism. As shown in Fig. 1, both SNNU-185 and SNNU-186 contain two distinct Co atoms that form two types of secondary building units (SBU I and SBU II). The Co_1 center is six-coordinated by four O-donors from four different 2,5-PDC ligands, one N-donor from TPB/TPP and one central μ_3-OH. Three Co_1 atoms form a $[Co_3(\mu_3\text{-OH})(COO)_6]$ trimer (Fig. 1a and b), acting as a 9-connected node. The Co_2 atom (Fig. 1c and d) is hexacoordinated in a distorted octahedral configuration formed by two carboxylate O and two pyridine N atoms from two 2,5-PDC ligands, and two N atoms from TPB/TPP ligands. Chelate rings are on the same side, forming $[Co(2,5\text{-PDC})_2(4\text{-pyridine})_2]$ MOLs (metal–organic linkers) in a *cis*-configuration, which is considered a 4-connected node. Two Co_1 trinuclear clusters and three Co_2 MOLs connect with each other to build a trigonal bipyramid-type cage along the *c*-axis, which is further extended into 1D $\{[Co_3(\mu_3\text{-OH})][Co(PDC)_2]_3\}_n$ chains (Fig. 1g).

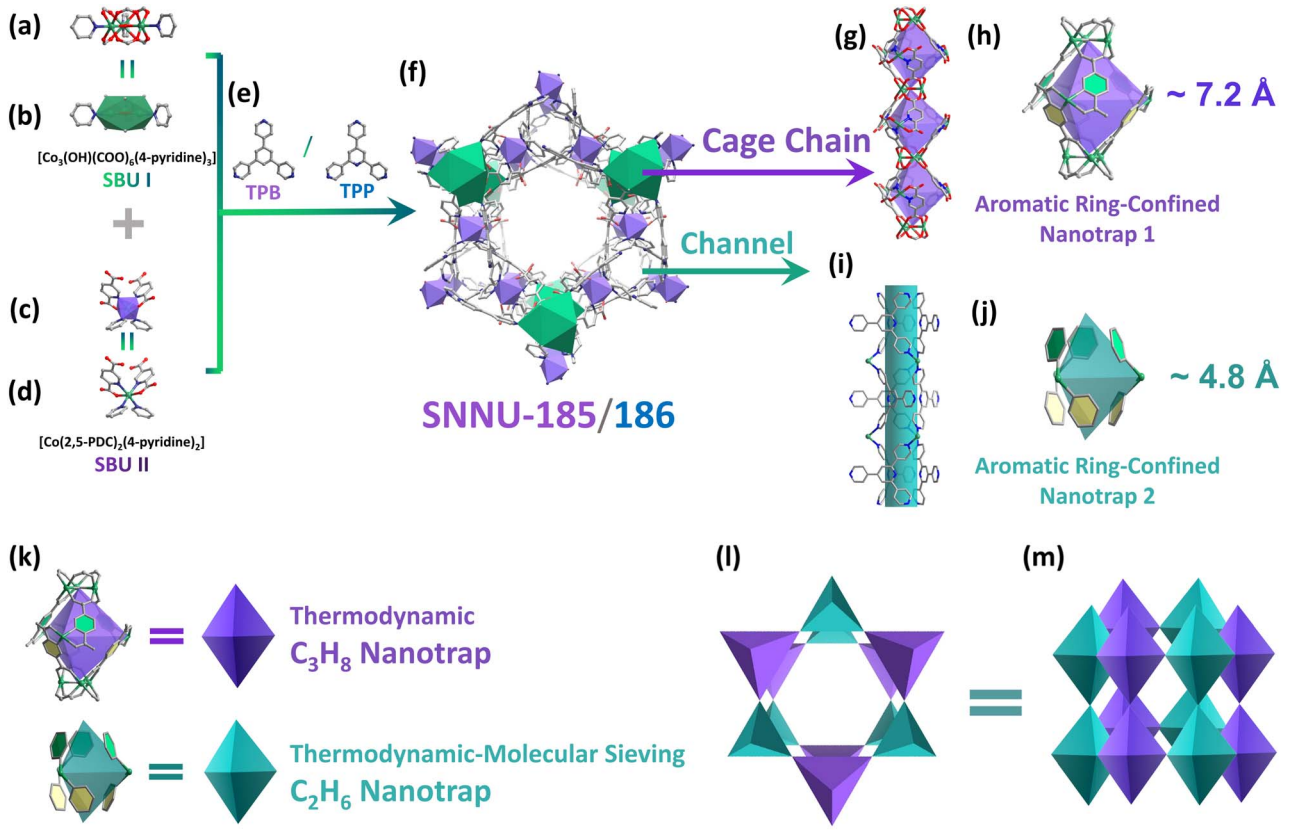

Fig. 1 Schematic representation showing the assembly of SNNU-185/186: (a–d) two types of clusters and their simplified representations in SNNU-185/186. (e) Triangular ligands TPB and TPP used to construct SNNU-185 and SNNU-186, respectively; (f) 3D structure of SNNU-185/186 viewed along the *c*-axis direction. Schematic diagram of nanotraps in (g) large-type nanotrap chains and (i) small-type nanotrap channels: (h) aromatic ring-confined nanotrap 1 and (j) aromatic ring-confined nanotrap 2 in SNNU-185/186. Schematic diagram of nanotraps: thermodynamic C_3H_8-selective nanotrap 1 and thermodynamic-molecular sieving C_2H_6-selective nanotrap 2. (k). Schematic diagram of 3D structures of SNNU-185/186 viewed along the (l) *c*-axis direction and (m) *b*-axis direction.

Significantly, each cage is decorated with six aromatic rings (from 2,5-PDC) and each aromatic ring layer has three aromatic rings which are distributed in a staggered pattern from top to bottom (Fig. 1h). The available inner cavity is ~7.2 Å × 7.2 Å and the window size is ~5.3 Å × 4.8 Å (Fig. 1h and S3c†). This cage size and environment match well with the size and shape of C_2H_6 and C_3H_8, acting as "aromatic ring-confined nanotrap 1" which is expected to promote the formation of strong host–guest interactions. Moreover, because the inner cavity of nanotrap 1 is more compatible with C_3H_8, this type of large nanotrap can act as C_3H_8-selective interaction sites. The 3D framework of SNNU-185/186 is formed when each cage chain connects six neighboring chains *via* six TPB/TPP ligands. The resulting small-sized channels (Fig. 1i) are also modified by six aromatic rings (from peripheral pyridine rings of TPB/TPP) in a staggered pattern from top to bottom, which are referred to as "aromatic ring-confined nanotrap 2" (Fig. 1j). This small nanotrap 2 has a pore size of about 4.8 Å × 4.8 Å and a window size of about 4.3 Å × 4.8 Å (Fig. S3d†). By summarizing and analyzing MOF materials with high C_2H_6/CH_4 separation performance such as Ni(TMBDC)(DABCO)$_{0.5}$ (ref. 2) (5.0 Å), ZUL-C_2 (ref. 4) (5.3 Å), Ni-MOF 1 (ref. 50) (5.7 Å), and SNNU-Bai$_{69}$ (ref. 3) (6.4 Å), it can be concluded that such pore sizes favor the formation of strong interactions with C_2H_6 through C–H···π bonds and can amplify the thermodynamic gap between C_2H_6 and CH_4 to the maximum extent. Furthermore, considering the size-exclusion potential of C_3H_8 as shown in KAUST-7,[51,52] Y-abtc,[53] Co-gallate,[54] JNU-3a,[55] and NTU-85-WNT[56] which have aperture sizes of about 4.7 Å, 4.7 Å, 5.2 Å, 5.3 Å and 4.6 Å respectively, this small-size channel is expected to limit C_3H_8 entry to some extent, thus creating C_2H_6-selective interaction sites based on a molecular sieving mechanism. Finally, the large channel decorated with oxygen atoms from uncoordinated carboxylic acids can also interact with gas molecules. However, considering its large pore size, the main role of the large channel might be to facilitate gas diffusion, allowing gas molecules to enter size-selective adsorption sites from pore walls. It can be concluded that the construction of C_2H_6-selective nanotraps, C_3H_8-selective nanotraps and mass transfer channels is achieved in SNNU-185 and SNNU-186 (Fig. 1k–m). Such a structural arrangement lays the foundation for efficient separation and recovery of C_2H_6 and C_3H_8 from natural gas.

PXRD patterns of the as-synthesized SNNU-185 and SNNU-186 samples align well with the calculated patterns obtained from the single crystals, indicating their successful synthesis with high purity (Fig. S6†). Also, a decagram scale synthesis of

SNNU-186 was carried out under reflux conditions for 3 days. As shown in Fig. S7 and S8,† impurity-free SNNU-186 (~12.7 g) could be easily obtained without loss of crystallinity, demonstrating its scalability. The TG analysis data showed that the as-synthesized and solvent-exchanged SNNU-185 and SNNU-186 are stable up to around 573 K, indicating their high thermal stability (Fig. S9†). Overall, the architecture of shape/size-matched bi-nanotraps, combined with size selectivity based on molecular sieving mechanisms and high stability inspired us to further investigate their $C_3H_8/C_2H_6/CH_4$ separation performance.

The permanent porosity of activated SNNU-185 and SNNU-186 was confirmed using N_2 adsorption–desorption isotherms at 77 K. As shown in Fig. S10,† both MOFs exhibit microporous type I sorption isotherms with calculated Brunauer–Emmett–Teller (BET) surface areas of 886 $m^2\ g^{-1}$ and 875 $m^2\ g^{-1}$ for SNNU-185 and SNNU-186, respectively. Single component adsorption isotherms for CH_4, C_2H_6, and C_3H_8 on SNNU-185 and SNNU-186 were measured at different temperatures (273, 283 and 298 K) and at pressures up to 1 bar (Fig. 2a, b and S11†). Taking advantage of the bi-nanotrap structure, SNNU-185/186 adsorbed much more C_3H_8 and C_2H_6 than CH_4 under the same conditions, indicating their potential for $C_3H_8/C_2H_6/CH_4$ separation. At 298 K and 1.0 bar, the C_2H_6 storage capacity of SNNU-185 and SNNU-186 can reach 69.8 $cm^3\ g^{-1}$ (3.12 mmol g^{-1}) and 74.3 $cm^3\ g^{-1}$ (3.32 mmol g^{-1}), respectively. These values exceed those of many well-known reported MOF adsorbents, such as Zn-BPZ-SA[5] (2.97 mmol g^{-1}), ZUL-C_1 (ref. 4) (2.95 mmol g^{-1}), ZUL-C_2 (ref. 4) (2.82 mmol g^{-1}), BSF-3 (ref. 38) (2.35 mmol g^{-1}), SNNU-Bai_{69} (ref. 3) (2.0 mmol g^{-1}), ECUT-Th-10a[11] (1.72 mmol g^{-1}) and UiO-66-Naph[34] (1.24 mmol g^{-1}). The C_3H_8 isotherms of SNNU-185 and SNNU-186 at 273/298 K exhibited saturated uptakes of 98.6/94.0 $cm^3\ g^{-1}$ (4.40/4.20 mmol g^{-1}) and 108.0/97.1 $cm^3\ g^{-1}$ (4.82/4.33 mmol g^{-1}), respectively, surpassing those of most MOF materials such as ZUL-C_1 (ref. 4) (2.72 mmol g^{-1}), ZUL-C_2 (ref. 4) (2.52 mmol g^{-1}), BSF-3 (ref. 38) (2.98 mmol g^{-1}), Ni-MOF 1 (ref. 50) (3.56 mmol g^{-1}) and LIFM-ZZ-1 (ref. 9) (4.06 mmol g^{-1}). Thanks to strong interactions from thermodynamic C_3H_8-selective nanotraps, the C_3H_8 uptake shows steep adsorption at low pressure, which is beneficial for capturing C_3H_8. For C_2H_6, steep adsorption at low pressure especially at 0–50 mm_{Hg} can also be observed, which might be attributed to strong interaction with C_2H_6-selective nanotraps. In addition, considering the presence of water and acidic gases such as H_2S and SO_2 in raw natural gas, detailed stability tests were further performed. After being treated under different conditions including soaking in water, exposure to aqueous solutions with different pH values or exposed to air for an extended period, satisfactory water stability and pH stability of these two MOFs were verified by adsorption/desorption tests (Fig. 2c).

To measure the binding affinities between the host surface and guest gas molecules, the adsorption enthalpy ($-Q_{st}$) of C_3H_8, C_2H_6 and CH_4 in SNNU-185/186 was calculated (Fig. 2d, S12 and Table S3†). Significantly, SNNU-186 shows the highest $-Q_{st}$ value of 48.8 kJ mol^{-1} for C_2H_6 compared to all reported

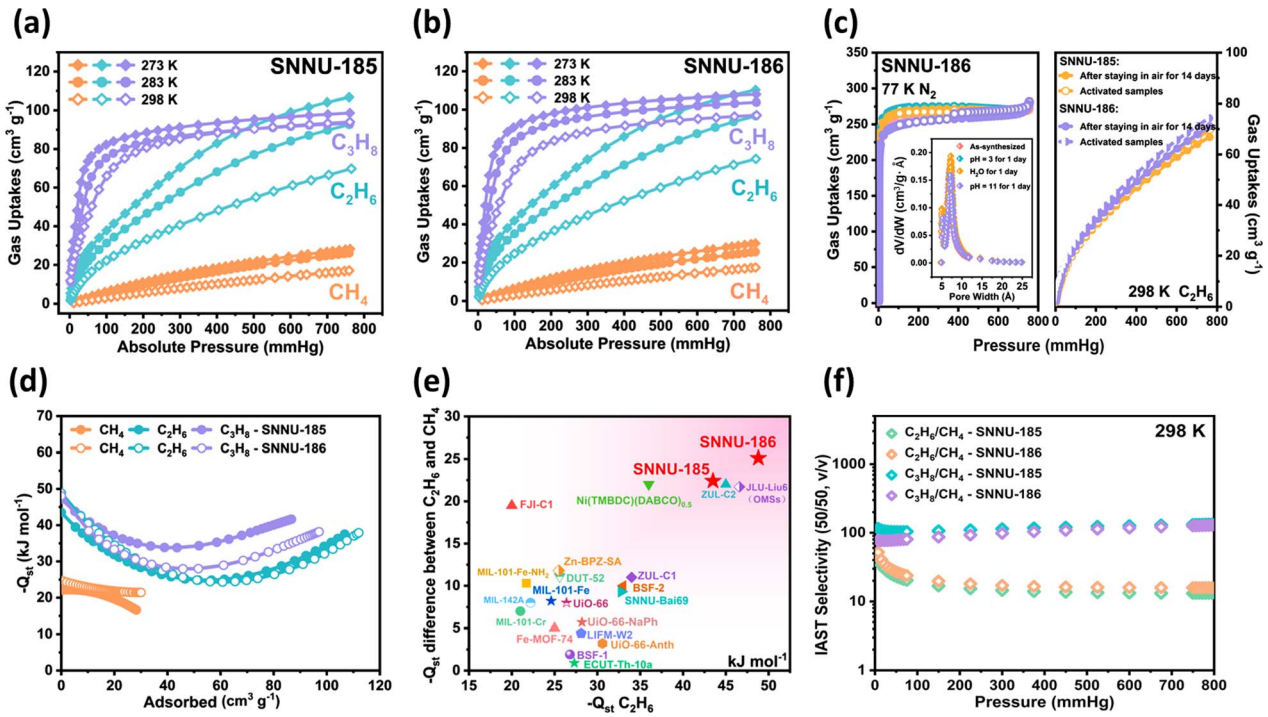

Fig. 2 C_3H_8, C_2H_6 and CH_4 sorption isotherms of (a) SNNU-185 and (b) SNNU-186 at 273/283/298 K. (c) Stability tests: 77 K N_2 adsorption/desorption isotherms and pore size distributions of SNNU-186 after being treated under different conditions, and C_2H_6 sorption isotherms of SNNU-185 and SNNU-186 before and after exposure to air for 14 days. (d) $-Q_{st}$ plots of C_3H_8, C_2H_6 and CH_4. (e) Summary of $-Q_{st}$ (C_2H_6) and the difference between $-Q_{st}$ (C_2H_6) and $-Q_{st}$ (CH_4) among all the reported MOF materials used for $C_3H_8/C_2H_6/CH_4$ separation. (f) IAST selectivity for C_2H_6/CH_4 mixtures (50/50) and C_3H_8/CH_4 mixtures (50/50) of SNNU-185 and SNNU-186 at 298 K.

MOF materials used for $C_3H_8/C_2H_6/CH_4$ separation such as ZUL-C_2 (ref. 4) (45 kJ mol^{-1}), Ni(TMBDC)(DABCO)$_{0.5}$ (ref. 2) (36 kJ mol^{-1}), ZUL-C1 (ref. 4) (33 kJ mol^{-1}) and SNNU-Bai$_{69}$ (ref. 3) (30.6 kJ mol^{-1}) (Table S4†). Importantly, SNNU-185 and SNNU-186 exhibit the largest $-Q_{st}$ difference between C_2H_6 and CH_4 among MOF materials used for natural gas upgrading (Fig. 2e). This benchmark $-Q_{st}$ for C_2H_6 and the largest thermodynamic interaction difference between C_2H_6 and CH_4 could be attributed to the bi-nanotrap structure which fully takes advantage of the synergistic effects of C–H$\cdots\pi$ interactions and nanotraps. As a result, multiple and strong C–H$\cdots\pi$ interactions and an increased thermodynamic interaction difference between gas molecules were achieved, which are beneficial for improving the performance in the key C_2H_6/CH_4 step. Due to strong C–H$\cdots\pi$ interactions in C_3H_8-nanotraps and the rejection of C_3H_8 by C_2H_6-nanotraps, the $-Q_{st}$ values for C_3H_8 in SNNU-185/186 are moderate (48.1/47.2 kJ mol^{-1}).

Ideal adsorbed solution theory (IAST) was used to further evaluate the separation potential of SNNU-185/186 for 50/50 C_2H_6/CH_4 mixtures and 50/50 C_3H_8/CH_4 mixtures at 298 K (Fig. 2f, S13–15 and Table S5†). At 1 kPa, for C_2H_6/CH_4, the IAST selectivities of SNNU-185 and SNNU-186 are 43.4 and 52.1, respectively. For 50/50 C_3H_8/CH_4, the selectivity values of SNNU-185 and SNNU-186 at 298 K and 100 kPa are 132.5 and 126.0, respectively. These values are not top-level but still higher than those of many well-known MOF materials, such as MIL-101-Cr[30] (84.3), ZUL-C_1 (ref. 4) (73), UiO-66 (ref. 34) (65) and ECUT-Th-10a[11] (54.5) under the same conditions.

Considering that the relatively small window size of the nanotraps might influence the gas diffusion behaviour, kinetic mass transfer factors were investigated. The adsorption kinetics of C_2H_6 and C_3H_8 were evaluated using the time-dependent uptake profile. As shown in Fig. S16,† both C_2H_6 and C_3H_8 with similar slopes could achieve complete desorption within similar timeframes, indicating their similar diffusion behaviour, thus excluding their diffusion rate differences as a key factor in their sorption properties. Demonstrating the extent of exclusiveness of bi-nanotraps is crucial and the key is to prove that C_2H_6 and C_3H_8 do not affect each other during the separation process. Since the selectivity of "bi-nanotraps" results from both "thermodynamics" and the "molecular sieving" mechanism rather than thermodynamics alone, and the effectiveness of "bi-nanotraps" in weakening competitive adsorption can be demonstrated when C_2H_6 and C_3H_8 coexist, two-component breakthrough tests were performed to provide evidence for the "bi-nanotrap" effect (Fig. 3a, b and S17–19†). As shown in Fig. 3a, whether mixed with CH_4 or C_2H_6, the breakthrough time of C_3H_8 was not affected ($\sim$115 min g^{-1}), implying that C_2H_6 does not affect the adsorption of C_3H_8. Moreover, whether mixed with CH_4 or C_3H_8, the breakthrough time of C_2H_6 was not affected ($\sim$62 min g^{-1}, Fig. 3b), implying that C_3H_8 does not affect the adsorption of C_2H_6 as well. Therefore, once gases enter the "bi-nanotrap" structure, it is expected that C_3H_8 will be adsorbed in C_3H_8-selective nanotrap 1 and C_2H_6 will be adsorbed in C_2H_6-selective nanotrap 2. Clearly, "bi-nanotraps" play a crucial role in removing the competitive adsorption between C_2H_6 and C_3H_8, thus improving $C_3H_8/C_2H_6/CH_4$ separation performance.

Inspired by the increased thermodynamic interaction difference and exclusive interaction sites, and encouraged by the satisfactory gas uptake and potential separation ability of activated SNNU-185/186, further experimental dynamic breakthrough experiments were performed to evaluate their $C_3H_8/C_2H_6/CH_4$ separation performance. As shown in Fig. 3c and S20,† CH_4 eluted out first due to its lowest adsorption capacity and weakest affinity with the frameworks, while C_2H_6 and C_3H_8 were trapped until their saturation sorption. For 20/80 C_2H_6/CH_4 and 20/80 C_3H_8/CH_4 mixtures with a total flow rate of 2 mL min^{-1} at 298 K, C_2H_6/C_3H_8 was retained for additional 66.0/204.0 min g^{-1} on SNNU-185, and 58.0/193.6 min g^{-1} on SNNU-186. Considering the practical composition of natural gas, experimental breakthrough tests with a feed gas of ternary $C_3H_8/C_2H_6/CH_4$ (5/10/85, v/v/v) mixtures at flow rates of 4/6 mL min^{-1} were carried out at 298 K. As shown in Fig. 3d–g and S21,† SNNU-185 and SNNU-186 can produce ultra-high purity CH_4 (>99.9999%) with exceptional productivities for CH_4. The CH_4 productivity of SNNU-185/186 was calculated to be 6.85/6.10 mmol g^{-1}, surpassing those of most top-performing MOFs such as SNNU-Bai$_{69}$ (ref. 3) (5.93 mmol g^{-1}), ZUL-C_1 (ref. 4) (5.42 mmol g^{-1}), BSF-1/2/3 (ref. 1, 14 and 38) (3.75/3.79/4.60 mmol g^{-1}), UiO-66-NaPh[34] (2.25 mmol g^{-1}), MIL-101-Cr[30] (2.66 mmol g^{-1}), and Zn-BPZ-SA[5] (1.56 mmol g^{-1}); it is comparable to that of MOF-303 (ref. 57) (7.97 mmol g^{-1}), and is only lower than those of ZUL-C_2 (ref. 4) (1 mL min^{-1}, 11.4 mmol g^{-1}) and Ni(TMBDC)(DABCO)$_{0.5}$ (ref. 2) (4 mL min^{-1}, 12.6 mmol g^{-1}) (Table S6†). When the experimental breakthrough tests were performed at a high flow rate of 6 mL min^{-1}, the CH_4 purity still reached 99.9999%, which can be attributed to the multiple interactions between C_2H_6 and MOF frameworks, as well as the increased interaction difference between C_2H_6 and CH_4.

Furthermore, considering the importance of C_2H_6 and C_3H_8 recovery, the breakthrough capture capacities of SNNU-185 and SNNU-186 for C_2H_6 and C_3H_8 were calculated accordingly. SNNU-185/186 possess outstanding C_2H_6 and C_3H_8 capture capacities of 1.23/0.90 mmol g^{-1} and 2.33/2.15 mmol g^{-1}, respectively, which are superior to those of most MOF materials and are comparable to those of top-level MOF materials such as ZUL-C_2 (ref. 4) (2.13/1.66 mmol g^{-1}), ZUL-C_1 (ref. 4) (0.98/1.19 mmol g^{-1}) and Ni-MOF 1 (ref. 50) (0.78/2.10 mmol g^{-1}) (Table S6†). As shown in Fig. 3h, when considering CH_4 productivity, breakthrough capture capacities for C_3H_8, and C_3H_8 uptake, SNNU-185 and SNNU-186 exhibit the best performance for CH_4 purification as well as for C_2H_6 and C_3H_8 recovery. Notably, the excellent separation performance of SNNU-185/186 is based on both "thermodynamics" and the "bi-nanotrap effect" in contrast to other MOFs that rely only on thermodynamics. As a result, although the thermodynamics-based IAST selectivities of SNNU-185/186 for C_2H_6/CH_4 are moderate, thanks to the guest-specific interactions, competitive adsorption between C_2H_6 and C_3H_8 is weakened and the practical separation performance is improved (Table S6†). Furthermore, considering the presence of CO_2 in raw natural gas and

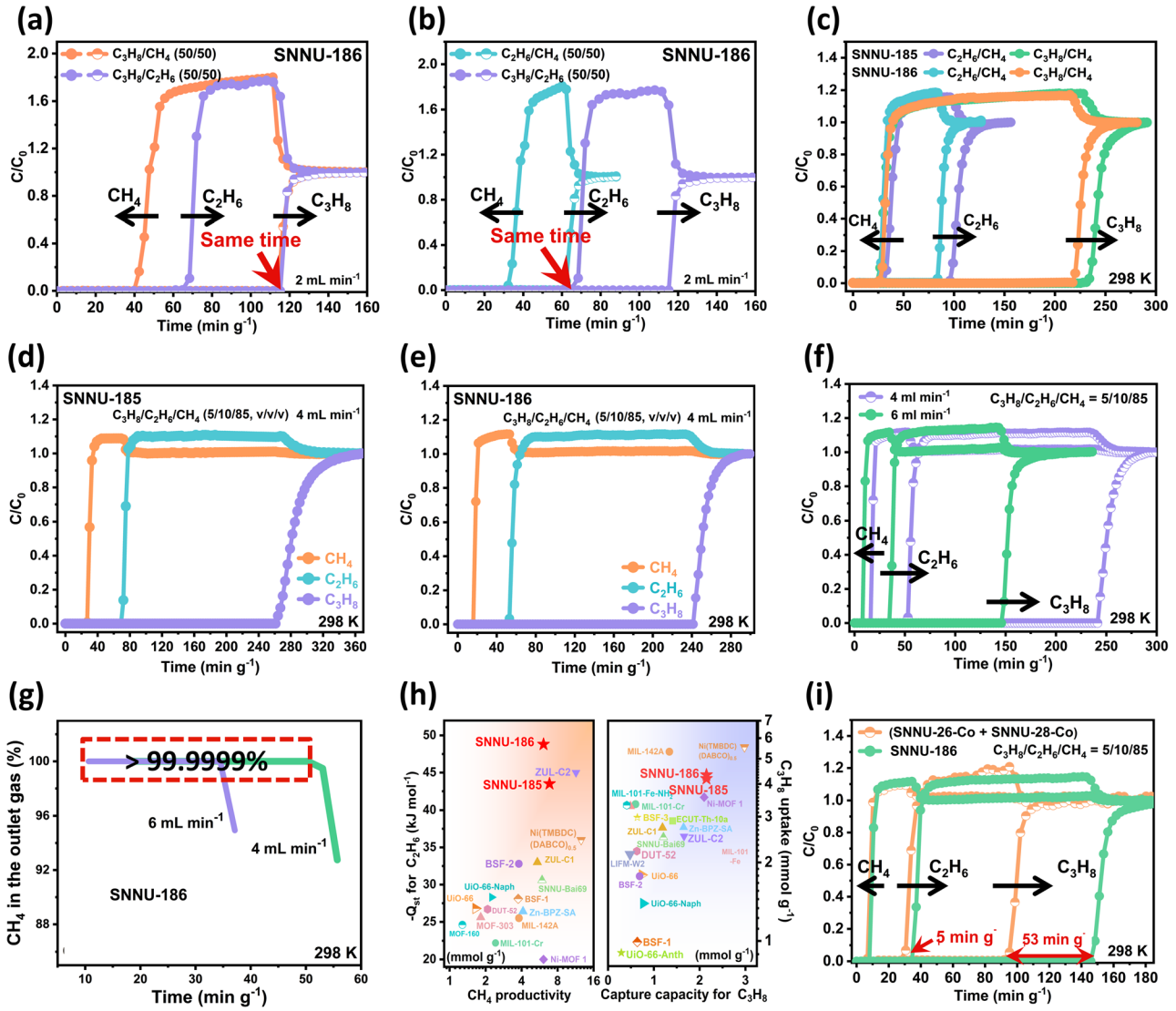

Fig. 3 Breakthrough curves for (a) C_3H_8/CH_4 (50/50, v/v) and C_3H_8/C_2H_6 (50/50, v/v) of SNNU-186 at 298 K; (b) C_2H_6/CH_4 (50/50, v/v) and C_3H_8/C_2H_6 (50/50, v/v) of SNNU-186 at 298 K; (c) C_2H_6/CH_4 (20/80, v/v) and C_3H_8/CH_4 (20/80, v/v) of SNNU-185 and SNNU-186; (d) $C_3H_8/C_2H_6/CH_4$ (5/10/85, v/v/v) of SNNU-185; (e) $C_3H_8/C_2H_6/CH_4$ (5/10/85, v/v/v) of SNNU-186; (f) $C_3H_8/C_2H_6/CH_4$ (5/10/85, v/v/v) of SNNU-186 with different total flow rates of 4 mL min^{-1} and 6 mL min^{-1}. (g) CH_4 purity in the $C_3H_8/C_2H_6/CH_4$ (5/10/85, v/v/v) outlet gas of SNNU-186. (h) Comparison of the separation performance among all reported MOFs used for $C_3H_8/C_2H_6/CH_4$ (5/10/85, v/v/v) separation. (i) Comparison of breakthrough curves of SNNU-186 and mixed MOFs (SNNU-26-Co + SNNU-28-Co) for $C_3H_8/C_2H_6/CH_4$ (5/10/85, v/v/v) with a total flow rate of 6 mL min^{-1}.

the challenges associated with its removal,[27] breakthrough experiments were conducted to provide an assessment of the impact of CO_2 contaminants. As shown in Fig. S22 and S23,† SNNU-186 could effectively separate $C_2H_6/CO_2/CH_4$ = 15/4/81 (v/v/v) and $C_3H_8/CO_2/CH_4$ = 4/4/92 (v/v/v) containing 4% CO_2. Overall, SNNU-185 and SNNU-186 are highly competitive candidates for natural gas upgrade.

Given that there are two types of pores in SNNU-185/186, comparative experiments were conducted to demonstrate the advantage of using a single material with two types of pores (~5 Å and ~7 Å) over using a mixture of two MOFs with one type of pore each. First, since many factors such as metal centers, open metal sites (OMSs), functional groups can strongly influence the adsorption behaviour of MOFs, it is necessary to ensure the same metal center (Co center) and a similar chemical environment (decorated with aromatic rings, N sites, no OMSs). Bearing the above factors in mind, two reported MOFs, SNNU-26-Co[58] (Co-BDC-TPP, with a pore size of ~5 Å) and SNNU-28-Co[58] (Co-2,6-NDC-TPP, with a pore size of ~7 Å) were selected (Table S7†). As shown in Fig. 3i and S24,† under the same conditions, SNNU-186 exhibited better practical separation performance, confirming that using one MOF with two types of pores is more favourable for the $C_3H_8/C_2H_6/CH_4$ separation process.

To give a mechanistic explanation of the role and effectiveness of the bi-nanotrap structure, and to gain a molecular-level insight into the host–guest interactions and adsorption behaviors of C_3H_8, C_2H_6 and CH_4, Grand Canonical Monte Carlo (GCMC) simulations were performed (Fig. 4 and S25†). As

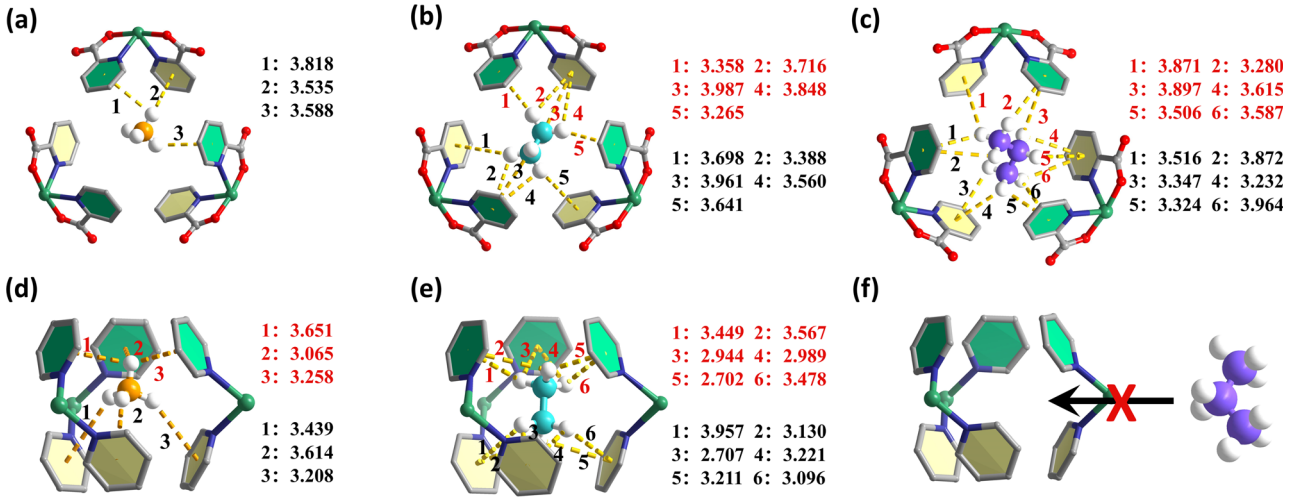

Fig. 4 GCMC simulated adsorption binding sites for (a) CH_4, (b) C_2H_6 and (c) C_3H_8 in nanotrap 1, (d) CH_4 and (e) C_2H_6 in nanotrap 2 and (f) the size limitation of nanotrap 2 for C_3H_8. The unit of interaction distance is angstrom (Å).

shown in Fig. 4a–c, the large-type nanotrap with a pore size of 7.2 Å can trap CH_4, C_2H_6 and C_3H_8 *via* multiple C–H···π bonds with distances between 3.535 Å and 3.818 Å (3 bonds) for CH_4, 3.265 Å and 3.987 Å (10 bonds) for C_2H_6, and 3.232 Å and 3.964 Å (12 bonds) for C_3H_8. Thanks to the higher number of H atoms in C_3H_8 and better size matching, these large nanotraps are more favorable for C_3H_8, forming more and stronger C–H···π bonds, and are thus considered thermodynamic C_3H_8-selective nanotraps. As for the small-type nanotraps with a pore size of 4.8 Å, they do not allow C_3H_8 molecules to enter due to the pore size limitation (Fig. 4d–f and S25†). However, C_2H_6 molecules can enter and bind to aromatic rings of TPP ligands on the surface of the nanotraps *via* a large number of strong and shape-matching C–H···π interactions with short distances (2.702–3.957 Å, 12 bonds), implying the exceptionally strong interactions between C_2H_6 and frameworks as well as preferential adsorption selectivity for C_2H_6 (Fig. 4e). As a result, C_2H_6-selective nanotraps are successfully constructed based on the dual integrated thermodynamic-molecular sieving mechanism. CH_4 molecules interact with both kinds of nanotraps *via* fewer and weaker interactions (Fig. 4a and d). Clearly, the construction of thermodynamic C_3H_8-selective nanotraps and coupled thermodynamic-molecular sieving C_2H_6-selective nanotraps in the bi-nanotrap structure provides a reasonable explanation for the benchmark performance of SNNU-185 and SNNU-186 for $C_3H_8/C_2H_6/CH_4$ separation. When C_2H_6 and C_3H_8 molecules coexist, they tend to preferentially occupy different and size-matching sites to form multiple and strong interactions, thus leading to a performance breakthrough.

Conclusions

In summary, a promising aromatic ring-confined bi-nanotrap strategy for excellent natural gas upgrading has been demonstrated here. The perfectly size/shape-matched C_2H_6-selective nanotraps and C_3H_8-selective nanotraps enable C_2H_6 and C_3H_8 to be preferentially trapped *via* abundant and extra-strong C–H···π bonds. Such a combination of thermodynamic-based nanotraps with molecular sieving-based size exclusion enables multiple, powerful and shape-matched interactions, and selective interaction sites, which is unprecedented. As a result, the goal of increasing the thermodynamic difference and reducing competitive adsorption was achieved. With excellent thermal/chemical stability and satisfactory gas sorption properties, the two MOFs reported here can produce high purity CH_4 at high flow rates along with achieving first-class productivities for CH_4, C_2H_6 and C_3H_8. This work not only creates highly ideal adsorbents with benchmark practical performance for natural gas upgrading, but also introduces a design concept of installing selective bi-nanotraps and fully exploiting the integrated thermodynamic-molecular sieving mechanism for the development of high-performance absorbents for more challenging multi-component gas systems.

Data availability

All the associated data are available in the ESI.†

Author contributions

Q.-G. Z. and S.-Y. L. conceived the idea of this research. S.-Y. L. carried out the experiments, analyzed the results and wrote the manuscript. Q.-G. Z. led the project and edited the manuscript. X. B. edited the manuscript. All authors participated in and contributed to the preparation of the manuscript.

Conflicts of interest

There are no conflicts to declare.

Acknowledgements

This work was financially supported by the National Natural Science Foundation of China (22071140), the Natural Science

Foundation of Shaanxi Province (2021JLM-20), the Youth Innovation Team of Shaanxi Universities (2023), and the Fundamental Research Funds for the Central Universities (GK202307009).

Notes and references

1 Y. Zhang, L. Yang, L. Wang, S. Duttwyler and H. Xing, *Angew. Chem., Int. Ed.*, 2019, **58**, 8145–8150.
2 Y. Wu, Z. Liu, J. Peng, X. Wang, X. Zhou and Z. Li, *ACS Appl. Mater. Interfaces*, 2020, **12**, 51499–51505.
3 M. Ding, Q. Wang, H. Cheng and J. Bai, *CrystEngComm*, 2022, **24**, 2388–2392.
4 J. Zhou, T. Ke, F. Steinke, N. Stock, Z. Zhang, Z. Bao, X. He, Q. Ren and Q. Yang, *J. Am. Chem. Soc.*, 2022, **144**, 14322–14329.
5 G.-D. Wang, R. Krishna, Y.-Z. Li, Y.-Y. Ma, L. Hou, Y.-Y. Wang and Z. Zhu, *ACS Mater. Lett.*, 2023, **5**, 1091–1099.
6 Y. He, W. Zhou, G. Qian and B. Chen, *Chem. Soc. Rev.*, 2014, **43**, 5657–5678.
7 J. Shen, A. Dailly and M. Beckner, *Microporous Mesoporous Mater.*, 2016, **235**, 170–177.
8 J. Li, X. Luo, N. Zhao, L. Zhang, Q. Huo and Y. Liu, *Inorg. Chem.*, 2017, **56**, 4141–4147.
9 Z. Zeng, W. Wang, X. Xiong, N. Zhu, Y. Xiong, Z. Wei and J.-J. Jiang, *Inorg. Chem.*, 2021, **60**, 8456–8460.
10 Z. Ke, H. Xiao, Y. Wen, S. Du, X. Zhou, J. Xiao and Z. Li, *Ind. Eng. Chem. Res.*, 2021, **60**, 4668–4676.
11 L. Wang, W. Zhang, J. Ding, L. Gong, R. Krishna, Y. Ran, L. Chen and F. Luo, *Nano Res.*, 2023, **16**, 3287–3293.
12 J.-R. Li, R. J. Kupplera and H.-C. Zhou, *Chem. Soc. Rev.*, 2009, **38**, 1477–1504.
13 K. Adil, Y. Belmabkhout, R. S. Pillai, A. Cadiau, P. M. Bhatt, A. H. Assen, G. Maurinb and M. Eddaoudi, *Chem. Soc. Rev.*, 2017, **46**, 3402–3430.
14 Y. Zhang, L. Yang, L. Wang, X. Cui and H. Xing, *J. Mater. Chem. A*, 2019, **7**, 27560–27566.
15 B. Li, M. Chrzanowski, Y. Zhang and S. Ma, *Coord. Chem. Rev.*, 2016, **307**, 106–129.
16 X. Zhao, Y. Wang, D.-S. Li, X. Bu and P. Feng, *Adv. Mater.*, 2018, **30**, 1705189.
17 E. D. Bloch, W. L. Queen, R. Krishna, J. M. Zadrozny, C. M. Brown and J. R. Long, *Science*, 2012, **335**, 1606–1610.
18 S. Yang, A. J. Ramirez-Cuesta, R. Newby, V. Garcia-Sakai, P. Manuel, S. K. Callear, S. I. Campbell, C. C. Tang and M. Schröder, *Nat. Chem.*, 2015, **7**, 121–129.
19 Q. Liu, S. G. Cho, J. Hilliard, T.-Y. Wang, S.-C. Chien, L.-C. Lin, A. C. Co and C. R. Wade, *Angew. Chem., Int. Ed.*, 2023, e202218854.
20 L. Wang, H. Huang, X. Zhang, H. Zhao, F. Li and Y. Gu, *Coord. Chem. Rev.*, 2023, **484**, 215111.
21 H.-C. Zhou, J. R. Long and O. M. Yaghi, *Chem. Rev.*, 2012, **112**, 673–674.
22 H.-C. Zhou and S. Kitagawa, *Chem. Soc. Rev.*, 2014, **43**, 5415–5418.
23 B. Li, H.-M. Wen, W. Zhou, J. Q. Xu and B. Chen, *Chem*, 2016, **1**, 557–580.
24 S. Rupam and C. D. Madhab, *Coord. Chem. Rev.*, 2021, **442**, 213998.
25 X. Han and S. Yang, *Angew. Chem., Int. Ed.*, 2023, e202218274.
26 H. Wang, D. Luo, E. Velasco, L. Yu and J. Li, *J. Mater. Chem. A*, 2021, **9**, 20874–20896.
27 P.-Q. Liao, W.-X. Zhang, J.-P. Zhang and X.-M. Chen, *Nat. Commun.*, 2015, **6**, 8697.
28 L. Li, R.-B. Lin, R. Krishna, H. Li, S. Xiang, H. Wu, J. Li, W. Zhou and B. Chen, *Science*, 2018, **362**, 443–446.
29 H. Zeng, X.-J. Xie, M. Xie, Y.-L. Huang, D. Luo, T. Wang, Y. Zhao, W. Lu and D. Li, *J. Am. Chem. Soc.*, 2019, **141**, 20390–20396.
30 L.-Z. Qin, X.-H. Xiong, S.-H. Wang, L. Zhang, L.-L. Meng, L. Yan, Y.-N. Fan, T.-A. Yan, D.-H. Liu, Z.-W. Wei and C.-Y. Su, *ACS Appl. Mater. Interfaces*, 2022, **14**, 45444–45450.
31 R.-B. Lin, H. Wu, L. Li, X.-L. Tang, Z. Li, J. Gao, H. Cui, W. Zhou and B. Chen, *J. Am. Chem. Soc.*, 2018, **140**, 12940–12946.
32 J. Pei, J.-X. Wang, K. Shao, Y. Yang, Y. Cui, H. Wu, W. Zhou, B. Li and G. Qian, *J. Mater. Chem. A*, 2020, **8**, 3613–3620.
33 Y. Ye, Y. Xie, Y. Shi, L. Gong, J. Phipps, A. M. Al-Enizi, A. Nafady, B. Chen and S. Ma, *Angew. Chem., Int. Ed.*, 2023, e202302564.
34 L. Zhang, X.-H. Xiong, L.-L. Meng, L.-Z. Qin, C.-X. Chen, Z.-W. Wei and C.-Y. Su, *J. Mater. Chem. A*, 2023, **11**, 12902–12909.
35 J. Peng, J. Zhong, Z. Liu, H. Xi, J. Yan, F. Xu, X. Chen, X. Wang, D. Lv and Z. Li, *ACS Appl. Mater. Interfaces*, 2023, **15**, 41466–41475.
36 Q. Dong, Y. Huang, K. Hyeon-Deuk, I.-Y. Chang, J. Wan, C. Chen, J. Duan, W. Jin and S. Kitagawa, *Adv. Funct. Mater.*, 2022, **32**, 2203745.
37 M. Wriedt, J. P. Sculley, A. A. Yakovenko, Y. Ma, G. J. Halder, P. B. Balbuena and H.-C. Zhou, *Angew. Chem., Int. Ed.*, 2012, **51**, 9804–9808.
38 L. Wang, W. Sun, S. Duttwyler and Y. Zhang, *J. Solid State Chem.*, 2021, **299**, 122167.
39 L. Yang, X. Cui, Q. Yang, S. Qian, H. Wu, Z. Bao, Z. Zhang, Q. Ren, W. Zhou, B. Chen and H. Xing, *Adv. Mater.*, 2018, **30**, 1705374.
40 O. T. Qazvini, R. Babarao, Z.-L. Shi, Y.-B. Zhang and S. G. Telfer, *J. Am. Chem. Soc.*, 2019, **141**, 5014–5020.
41 Z. Niu, X. Cui, T. Pham, P. C. Lan, H. Xing, K. A. Forrest, L. Wojtas, B. Space and S. Ma, *Angew. Chem., Int. Ed.*, 2019, **58**, 10138–10141.
42 Y.-Y. Xue, S.-N. Li, Y.-C. Jiang, M.-C. Hu and Q.-G. Zhai, *J. Mater. Chem. A*, 2019, **7**, 4640.
43 Z. Niu, X. Cui, T. Pham, G. Verma, P. C. Lan, C. Shan, H. Xing, K. A. Forrest, S. Suepaul, B. Space, A. Nafady, A. M. Al-Enizi and S. Ma, *Angew. Chem., Int. Ed.*, 2021, **60**, 5283–5288.
44 Y. Ye, S. Xian, H. Cui, K. Tan, L. Gong, B. Liang, T. Pham, H. Pandey, R. Krishna, P. C. Lan, K. A. Forrest, B. Space, T. Thonhauser, J. Li and S. Ma, *J. Am. Chem. Soc.*, 2022, **144**, 1681–1689.

45 H. Zhu, Y. Wang, X. Wang, Z.-W. Fan, H.-F. Wang, Z. Niu and J.-P. Lang, *Chem. Commun.*, 2023, **59**, 5757.
46 Y. Wang, N.-Y. Huang, X.-W. Zhang, H. He, R.-K. Huang, Z.-M. Ye, Y. Li, D.-D. Zhou, P.-Q. Liao, X.-M. Chen and J.-P. Zhang, *Angew. Chem., Int. Ed.*, 2019, **58**, 7692–7696.
47 L. Yang, S. Qian, X. Wang, X. Cui, B. Chen and H. Xing, *Chem. Soc. Rev.*, 2020, **49**, 5359–5406.
48 F. Zheng, R. Chen, Z. Zhang, Q. Yang, Y. Yang, Q. Ren and Z. Bao, *Cell Rep. Phys. Sci.*, 2022, **3**, 100903.
49 Y.-Y. Xue, S.-N. Li, Y.-C. Jiang, M.-C. Hu and Q.-G. Zhai, *J. Mater. Chem. A*, 2019, **7**, 4640.
50 X.-X. Zhang, X.-Z. Guo, S.-S. Chen, H.-W. Kang, Y. Zhao, J.-X. Gao, G.-Z. Xiong and L. Hou, *Chem. Eng. J.*, 2023, **466**, 143170.
51 A. Cadiau, K. Adil, P. M. Bhatt, Y. Belmabkhout and M. Eddaoudi, *Science*, 2016, **353**, 137–140.
52 Y. Cheng, B. Joarder, S. J. Datta, N. Alsadun, D. Poloneeva, D. Fan, R. Khairova, A. Bavykina, J. Jia, O. Shekhah, A. Shkurenko, G. Maurin, J. Gascon and M. Eddaoudi, *Adv. Mater.*, 2023, 2300296.
53 H. Wang, X. Dong, V. Colombo, Q. Wang, Y. Liu, W. Liu, X.-L. Wang, X.-Y. Huang, D. M. Proserpio, A. Sironi, Y. Han and J. Li, *Adv. Mater.*, 2018, **30**, 1805088.
54 B. Liang, X. Zhang, Y. Xie, R.-B. Lin, R. Krishna, H. Cui, Z. Li, Y. Shi, H. Wu, W. Zhou and B. Chen, *J. Am. Chem. Soc.*, 2020, **142**, 17795–17801.
55 H. Zeng, M. Xie, T. Wang, R.-J. Wei, X.-J. Xie, Y. Zhao, W. Lu and D. Li, *Nature*, 2021, **595**, 542–548.
56 Q. Dong, Y. Huang, J. Wan, Z. Lu, Z. Wang, C. Gu, J. Duan and J. Bai, *J. Am. Chem. Soc.*, 2023, **145**, 8043–8051.
57 S. Xian, J. Peng, H. Pandey, T. Thonhauser, H. Wang and J. Li, *Engineering*, 2023, **23**, 56–63.
58 Y.-Y. Xue, X.-Y. Bai, J. Zhang, Y. Wang, S.-N. Li, Y.-C. Jiang, M.-C. Hu and Q.-G. Zhai, *Angew. Chem., Int. Ed.*, 2021, **60**, 10122–10128.